https://doi.org/10.1016/j.nima.2020.164103

Modelling and performance analysis of a GaN-based n/p junction betavoltaic cell

F. Bouzid[1,*], L. Dehimi[2], F. Pezzimenti[3],

[1]Research Center in Industrial Technologies CRTI, P.O. Box 64,Cheraga 16014, Algiers, Algeria.

[2]Faculty of Science, University of Batna, Batna 05000, Algeria.

[3]DIIES – Mediterranea University of Reggio Calabria, 89122 Reggio Calabria, Italy.

[*]E-mail Address: f.bouzid@crti.dz

Abstract

In this work, we optimized the performance of a gallium nitride (*GaN*)-based *n/p* junction betavoltaic cell irradiated by the radioisotope nickel-63 (Ni^{63}). In particular, we developed a lab-made software starting from an analytical model that takes into account a set of fundamental physical parameters for the cell structure. The simulations reveal that, by using a Ni^{63} radioisotope source with a 25 mCi/cm² activity density emitting a flux of beta-particles with an average energy of 17.1 KeV, the cell performs a conversion efficiency (η) in excess of 26%, thus approaching the theoretical limit for a *GaN*-based device. The other electrical parameters of the cell, namely the short-circuit current density (J_{sc}), open-circuit voltage (V_{oc}), and maximum electrical power density (P_{max}) are 240 nA/cm², 2.87 V, and 660 nW/cm², respectively. The presented analysis can turn useful for understanding the theoretical background needed to better face *GaN*-based betavoltaic cell design problems.

Keywords- Analytical modelling, gallium nitride, betavoltaic cell, nickel-63 radioisotope, radioactivity density.

1. Introduction

With the continuous development in technology and human lifestyle, the interest in long-

life power batteries has significantly increased in recent years. Nowadays, based on their energy source, batteries can be divided into three major groups, namely chemical, solar, and nuclear. After rigorous theoretical and experimental studies, it was clear that the possibilities of the first and second categories are limited in many applications with respect to the enormous and attractive potential of the nuclear approach. For example, we can consider all the applications where battery replacement is inconvenient or impossible such as implantable prosthetic devices, automatic weather stations in the arctic, deep-sea explorations, space missions, and so on.

Nuclear batteries converts the kinetic energy of alpha- or beta-particles, which is emitted from a radioactive isotope source, into electrical energy across semiconductor materials similarly to the solar cell working principle. Accordingly, they are called alphavoltaic or betavoltaic cells. The right choice of the radioactive source, as well as the absorbing semiconductor material, depends on many factors among which we can quote the radioisotope half-life fitting the task duration, decay type, and energy content. At the same time, the semiconductor material must have both good radiation resistance and high conversion efficiency. In this context, by considering the high penetration ability of beta-particles and the less radiation damage that attains the device structure if compared to the use of alpha-particle, the development and exploitation of betavoltaic cells have gained a great attention.

The concept of nuclear batteries was suggested by *Mosely* in 1913 and the first betavoltaic design based on silicon *p*/*n* junctions was investigated by *Rappaport* in the ‘50s [1,2]. Since 1989, the development of betavoltaic batteries has involved the use of alternative semiconductor compounds such as gallium arsenide (*GaAs*) [3,4], silicon carbide (*SiC*) [5-8], gallium nitride (*GaN*) [9-11], aluminium gallium arsenide (*AlGaAs*) [12,13], and indium gallium phosphide (*InGaP*) [14,15]. Different devices based in turn on *p*/*n*, *p*-*i*-*n*, and *Schottky* structures were designed to exploit the advantages of radioisotopes that emit beta-particles [16-

22]. Also, a great improvement in performance has been achieved thanks to the efforts in theoretical research based on analytical and/or numerical simulations, which contribute significantly in gaining time and limiting the financing required for experimental tasks involving relatively dangerous and expensive materials [23-28].

Within this framework, considering the need for more understanding how different physical and geometrical parameters of a wide bandgap material like *GaN* affect the performance of a nuclear battery, we have developed a comprehensive analytical model and compiled a lab-made software that allows an exhaustive analysis of a *GaN*-based *n*/*p* junction betavoltaic cell irradiated by the radioisotope nickel-63 (Ni^{63}). In more detail, by using a set of reference parameters for simulations, in this paper we have investigated the effects of the doping concentration, surface recombination velocity, junction depth, reflection coefficient, and Ni^{63} radioactivity density in determining the optimal performance of the cell. In particular, moving from the current density-voltage characteristics, we have extracted the main figures of merit of the cell, namely the short-circuit current density (J_{sc}), open-circuit voltage (V_{oc}), maximum power density (P_{max}), and conversion efficiency (η). This latter parameter results, in particular, very close to the device theoretical limit.

2. Theoretical background

In the design of a betavoltaic cell, the radioactive source must be carefully chosen taking into account the fact that the maximum kinetic energy (E_{max}) of beta-particles should be smaller than the semiconductor radiation damage threshold [29]. Currently, beta-sources which have proven their effectiveness are mainly tritium (H^3), nickel (Ni^{63}), and promethium (Pm^{147}). A comparison between the physical properties of different radioisotopes is summarized in Table 1 [1].

https://doi.org/10.1016/j.nima.2020.164103

Table 1 Physical properties of different beta-particles.

Isotope	Half-life (Years)	E_{max}(KeV)	E_{av} (KeV)	Radio toxicity
Pm^{147}	2.6	224	61.93	High
Co^{60}	5.3	318	96	High
H^{3}	12.32	18.6	5.68	Low
Sr^{90}	28.8	546	195.8-196.4	High
Cs^{137}	30.1	1175	416.3	High
Ni^{63}	100.1	65.9	17.1-17.4	Low

As we can see, for betavoltaic batteries, the use of Ni^{63} is preferable due to its long half-life, pure beta-particle emission, and relatively low beta-particle energy which results in a low radiation induced defect concentration in the semiconductor converter. In addition, Ni^{63} can be used also to form the electrodes of betavoltaic cells based on Schottky contacts. Likewise, to design high efficient cells, the semiconductor structure must perform high radiation hardness, low leakage current, high thermal conductivity, good electronic mobility, and long minority carrier diffusion lengths.

Recently, interest in wide bandgap materials such as *GaN* and *SiC* has been increased constantly in different fields [30-38]. The performance of several *GaN*- and *SiC*-based betavoltaic cells is reported in Table 2.

GaN with its wide bandgap of 3.39 eV seems to be the more attractive choice to design the next generation of betavoltaic cells [39]. In addition, it is worthwhile noting that the theoretical efficiency limits for *GaN* is close to 28% [40].

https://doi.org/10.1016/j.nima.2020.164103

Table 2 Performance of several betavoltaic cells based on *GaN* and *SiC*.

Material	Structure	Radioisotope	Activity (mCi)	Efficiency (%)	Ref.
SiC	*Schottky*	Am^{241}	0.018	0.1	[19]
SiC	p-i-n	Kr^{85}	1200	0.75-1.15	[5]
SiC	p-n	Ni^{63}	-	3.08	[7]
SiC	p-i-n	Ni^{63}	0.16	1.99	[20]
4H-SiC	*Schottky*	Ni^{63}	0.12	1.01	[6]
SiC	*Schottky*	Ni^{63}	2.7	6	[24]
4H-SiC	p-n	TiH^{3}	14.97	18.6	[8]
GaN	p-n	Ni^{63}	1	8.25	[26]
GaN	p-i-n	Ni^{63}	2	1.13	[28]
GaN	p-i-n	Ni^{63}	-	1.6	[9]
GaN	p-i-n	Ni^{63}	32.4	0.016	[27]
GaN	Double p-n	Ni^{63}	-	25.4	[18]
GaN	Double p-n	Ni^{63}	-	25	[21]
GaN	*Schottky*	Ni^{63}	3.3	0.32	[10]
GaN	*Schottky*	Ni^{63}	2.7	13	[24]
GaN	p-i-n	Ni^{63}	12.5	0.21	[23]
GaN	p-i-n	Ni^{63}	0.5	2.7	[22]
GaN	p-n	Ni^{63}	0.31	0.05	[11]

3. Model description

3.1. Theoretical basis

The schematic structure of the betavoltaic cell investigated in this work is shown in Fig. 1 (plot not to scale). The structure consists of a 1 cm² active area of *GaN* coupled with a beta-emitting Ni^{63} radioisotope source assuming that the kinetic energy ranges from 0 to 66.7 KeV with an average value of 17.1 KeV. The *n*-doped region represents the emitter while the *p*-doped region is the base. In Fig. 1, H is the whole cell thickness, namely the maximum beta-particles penetration depth, x_j is the junction depth, and H' is defined as:

$$H' = H - \left(x_j + W\right) \tag{1}$$

https://doi.org/10.1016/j.nima.2020.164103

where W is the depletion region width. In accordance with previous results reported in literature [9,41,42], the reference value of H is assumed equal to 1.5 μm.

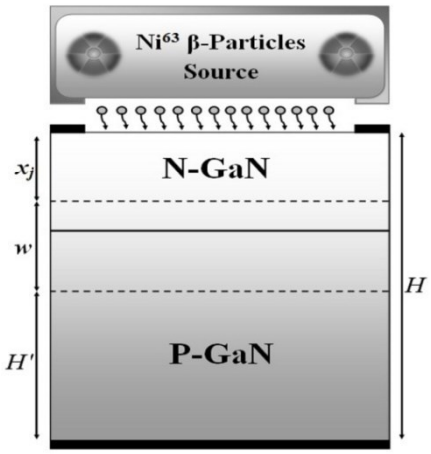

Fig.1 Schematic cross-section of the studied GaN-based betavoltaic cell.

When beta-particles pass through the structure, they will generate electron-hole pairs (*EHPs*) within the different regions by ionization phenomena. The output current produced by the cell is therefore proportional to the total number of absorbed electrons. The average energy required to form one *EHP* for both direct and indirect bandgap semiconductors is given by the empirical formula [1]:

$$\varepsilon(eV) = 2.67 \times E_g + 0.87 \tag{2}$$

where E_g is the temperature-dependent bandgap energy.

The adopted model for describing the cell operation is the single diode model. Similar to the solar cell structure, when a load resistor is connected to the terminals of a betavoltaic cell under irradiation, a voltage drop is developed and the total amount of the device output current density is calculated as [43]

$$J_{Total} = J_{Rad} - J_D \tag{3}$$

where J_{Rad} is the current density generated by the incident beta-particles radiation and J_D is the diode current component described by the standard expression:

https://doi.org/10.1016/j.nima.2020.164103

$$J_D = J_0\left[e^{\frac{qV}{nkT}} - 1\right] \tag{4}$$

where V is the biasing voltage, k is Boltzmann's constant, T is the temperature, q is the electron charge, n is the ideality factor, and J_0 is the reverse saturation current given by [44]

$$J_0 = \frac{qD_n n_i^2}{L_n N_a} \times \frac{\frac{S_n L_n}{D_n}\cosh(\frac{H'}{L_n}) + \sinh(\frac{H'}{L_n})}{\frac{S_n L_n}{D_n}\sinh(\frac{H'}{L_n}) + \cosh(\frac{H'}{L_n})} + \frac{qD_p n_i^2}{L_p N_d} \times \frac{\frac{S_p L_p}{D_p}\cosh(\frac{x_j}{L_p}) + \sinh(\frac{x_j}{L_p})}{\frac{S_p L_p}{D_p}\sinh(\frac{x_j}{L_p}) + \cosh(\frac{x_j}{L_p})} \tag{5}$$

Here, $N_{d,a}$ are the donor and acceptor doping concentrations, $S_{n,p}$ are the minority carrier surface recombination velocities, $L_{n,p}$ are the carrier diffusion lengths, $D_{n,p}$ are the carrier diffusion constants, and n_i is the intrinsic carrier concentration.

In (3), the current density J_{Rad}, which represents the current generated by the radiation under the short-circuit condition (V = 0), is calculated as the sum of three current density contributions. In particular, J_{Rad} accounts for the current capabilities of the quasi-neutral regions in the emitter (J_E) and in the base (J_B) of the cell as well as in the depletion region (J_{DR}). These current components are in the form of [45,46]

$$J_E = \left[\frac{N_\beta q E_k (1-R)\alpha L_p}{\varepsilon\left(\alpha^2 L_p^2 - 1\right)}\right] \times \left[\frac{\left(\frac{S_p L_p}{D_p} + \alpha L_p\right) - e^{-\alpha x_j}\left(\frac{S_p L_p}{D_p}\cosh\frac{x_j}{L_p} + \sinh\frac{x_j}{L_p}\right)}{\left(\frac{S_p L_p}{D_p}\sinh\frac{x_j}{L_p} + \cosh\frac{x_j}{L_p}\right)} - \alpha L_p e^{-\alpha x_j}\right] \tag{6}$$

$$J_B = \left[\frac{N_\beta q E_k (1-R)\alpha L_n}{\varepsilon\left(\alpha^2 L_n^2 - 1\right)} e^{-\alpha\left(x_j + W\right)}\right] \times \left[\alpha L_n - \frac{\frac{S_n L_n}{D_n}\left[\cosh\frac{H'}{L_n} - e^{-\alpha H'}\right] + \sinh\frac{H'}{L_n} + \alpha L_n e^{-\alpha H'}}{\left(\frac{S_n L_n}{D_n}\sinh\frac{H'}{L_n} + \cosh\frac{H'}{L_n}\right)}\right] \tag{7}$$

https://doi.org/10.1016/j.nima.2020.164103

$$J_{DR} = \frac{N_\beta q E_k (1-R)}{\varepsilon} e^{-\alpha x_j} \left(1 - e^{-\alpha W}\right) \tag{8}$$

where E_k is the kinetic energy of beta-particles, α is the absorption coefficient, N_β is the incident flux of beta-particles, and R is the reflection coefficient [47].

The key physical models and reference parameters taken into account during the simulations are summarized in Table 3 [48-53].

Table 3 GaN physical models and reference parameters.

Bandgap energy	$E_g(T) = E_{g300} + \alpha\left(\frac{300^2}{300+\beta} - \frac{T^2}{T+\beta}\right)$	E_{g300} = 3.39 eV α = 9.39 × 10^{-4} eV/K β = 772
Carrier lifetime	$\tau_{n,p} = \frac{\tau_{0n,p}}{1 + \left(\frac{N}{N_{n,p}^{SRH}}\right)}$	$\tau_{0n,p}$ = 0.5 ns $N_{n,p}^{SRH}$ = 5×10^{16} cm^{-3}
Carrier mobility	$\mu_{n,p} = \mu_{n,p}^{\min} + \frac{\mu_{n,p}^{\max}\left(\frac{T}{300}\right)^{\alpha} - \mu_{n,p}^{\min}}{1 + \left(\frac{T}{300}\right)^{\beta}\left(\frac{N}{N_{n,p}^{ref}}\right)^{\gamma}}$	$\mu_n^{\min}$ =55 $cm^2/V{\cdot}s$ $\mu_p^{\min}$ = 30 $cm^2/V{\cdot}s$ $\mu_n^{\max}$ =1418 $cm^2/V{\cdot}s$ $\mu_p^{\max}$ =175 $cm^2/V{\cdot}s$ N_n^{ref} = 2×10^{17} cm^{-3} N_p^{reft} = 3×$10^{17}$$cm^{-3}$ α_n = -2, α_p = -3 β_n = -3.8, β_p = -3.7 γ_n = 1, γ_p = 2
Intrinsic carrier concentration	$n_i = \sqrt{N_c N_v} e^{-\frac{E_g}{2kT}}$	N_V = 2.50×10^{19} cm^{-3} N_C = 2.65×10^{18} cm^{-3}
Depletion width	$W = \left[\frac{2\varepsilon_0 \varepsilon_r V_d (N_a + N_d)}{q N_a N_d}\right]^{0.5}$	ε_r = 9.5
Built-in potential	$V_d = \frac{kT}{q} \ln\left(\frac{N_a N_d}{n_i^2}\right)$	T = 300 K n_i = 1.07×10^{-10} cm^{-3}

https://doi.org/10.1016/j.nima.2020.164103

3.2. Calculation of the cell electrical properties

The open-circuit voltage and short-circuit current density are important parameters which describe the performance of the cell. In more detail, V_{oc} represents the largest voltage that can be produced between the cell electrodes by assuming $J_{Total} = 0$ in (3), i.e.

$$V_{oc} = \frac{nkT}{q} \times \ln\left(\frac{J_{sc}}{J_0} + 1\right) \tag{9}$$

where $J_{sc} = J_{Rad}$ is the current density generated by the betavoltaic cell under irradiation when its contacts are short-circuited.

From the $J(V)$ characteristics of the cell, another important parameter is the output power delivered to a load resistor, i.e.

$$P = J_{Total} \times V \tag{10}$$

Once finding the total electric power $P(V)$, its maximum value (P_{max}) is extracted by solving $dP/dV = 0$. Finally, the maximum conversion efficiency (η) of the betavoltaic cell is defined as the ratio

$$\eta = \frac{P_{\max}}{P_{inc}} = \frac{J_{MPP} \times V_{MPP}}{P_{inc}} \tag{11}$$

where P_{inc} is the input power density of the incident beta-particles in the form of [54,55]

$$P_{inc} = 3.7 \times 10^{10} \times qAZE_{av} \tag{12}$$

where A is the activity density of the radioisotope source, E_{av} is the average energy of beta-particles, and $Z = 1$ is a decay mode coefficient [19,56].

4. Results and discussion

4.1 Doping concentration effect

In order to find-out the optimal doping concentrations of the *n* and *p* regions of the cell, we

https://doi.org/10.1016/j.nima.2020.164103

simulated the $J(V)$ characteristics for a wide range of the terms N_d and N_a.

By assuming the physical and geometrical parameters listed in Table 4 as entry data for modelling, and by fixing the radioactivity density and the beta-particle average energy at 1 mCi/cm² and 17.1 KeV, respectively, the obtained results are shown in Figs.2 and 3.

Table 4 Entry data for modelling.

***T* (K)**	***Eg* (eV)**	***α*(cm^{-1})**	***S$_p$*(cm/s)**	***S$_n$*(cm/s)**
300	3.39	10^5	5×10^3	5×10^3
***x$_j$*(μm)**	***H*(μm)**	***R***	***n***	***S*(cm²)**
0.2	1.5	0.05	1.15	1

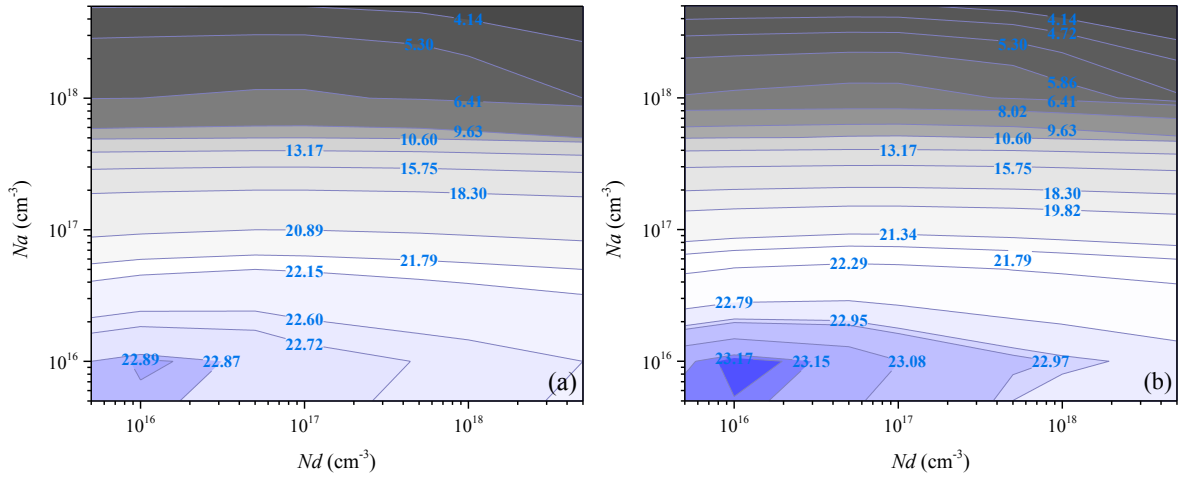

Fig. 2 (a)- η , (b)- P_{max}, of the *GaN*-based betavoltaic cell as a function of N_d and N_a at $T = 300$ K.

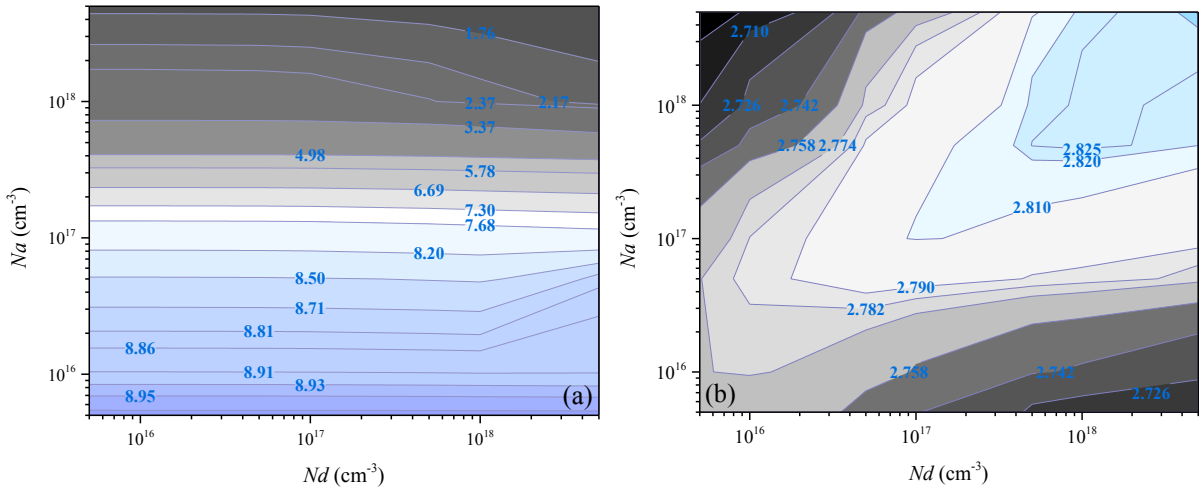

Fig. 3 (a)- J_{sc}, (b)-V_{oc}, of the *GaN*-based betavoltaic cell as a function of N_d and N_a at $T = 300$ K.

Here, it is clearly shown that the optimum doping concentration is close to 1×10^{16} cm^{-3} for both the donor- and acceptor-type, reaching the cell a conversion efficiency of 22.89%. Under this condition, P_{max}, J_{sc}, and V_{oc} are calculated as 23.17 nW/cm², 8.91 nA/cm² and 2.77 V, respectively.

In more detail, the conversion efficiency behaviour with changing the doping concentration can be explained through the analysis of the terms J_{sc}, and V_{oc}. In particular, high doping concentrations result in a smaller minority carrier diffusion length and also in a reduction of the depletion region width. Therefore, the adoption of low doping concentrations certainly enhances the collection of a high carrier charge density related to the wider depletion region, and the terms J_{sc}, P_{max}, and η increase accordingly. On the other hand, according to (9), V_{oc} mainly depends on the ratio J_{sc}/J_0 and considering the reverse proportionality that exists between J_0 and the doping concentrations in (5), V_{oc} increases with increasing the doping concentration as verified in Fig. 3(b). The adopted value of the doping concentration is consistent with literature [22,26].

4.2 Surface recombination velocity effect

Likewise the other optoelectronic devices, the surface of a betavoltaic cell can contain many sites of impurities into the crystal lattice where several recombination processes occur. In particular, the surface recombination velocity (S_p) has a major impact on the cell performance. In fact, high S_p values have a particularly harmful impact on the electrical parameters of the cell since the top surface corresponds to the highest generation region of carriers.

In Fig. 4, different $J(V)$ characteristics are plotted for a back surface recombination velocity fixed at 5×10^3 cm/s and a surface recombination velocity ranging from 10^3 cm/s to 10^5 cm/s to

https://doi.org/10.1016/j.nima.2020.164103

account for different treatments during the fabrication process. The influence of changing S_p on the electrical parameters P_{max}, η, J_{sc}, and V_{oc} is shown in Figs. 5 and 6.

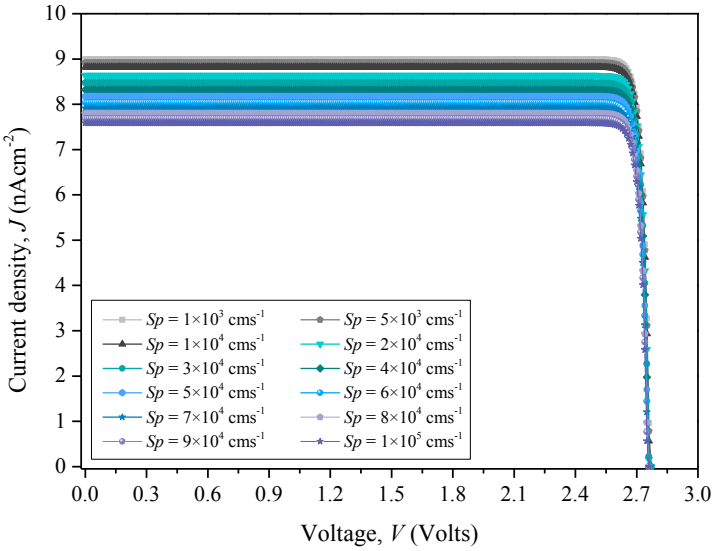

Fig. 4 Influence of the surface recombination velocity S_p on the $J(V)$ characteristics of the *GaN*-based betavoltaic cell at $T = 300$ K.

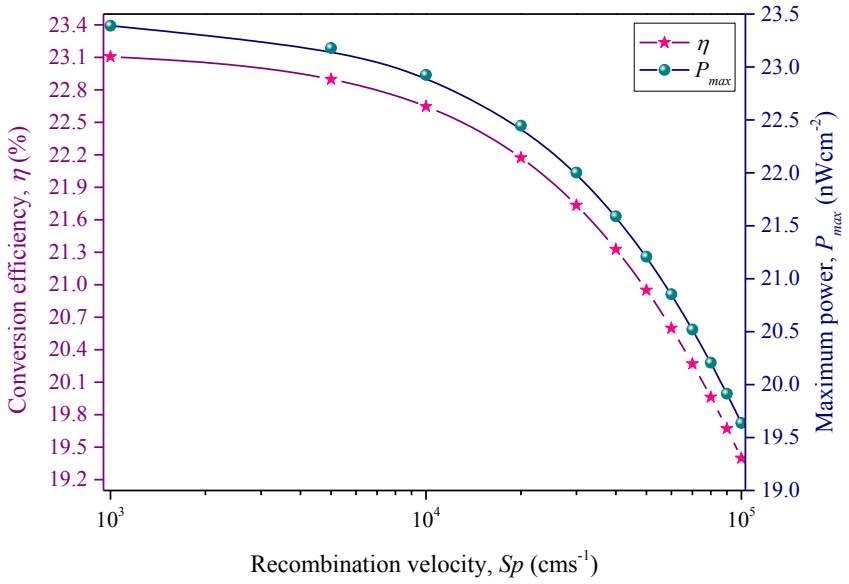

Fig. 5 Evolution of η and P_{max} as a function of S_p.

https://doi.org/10.1016/j.nima.2020.164103

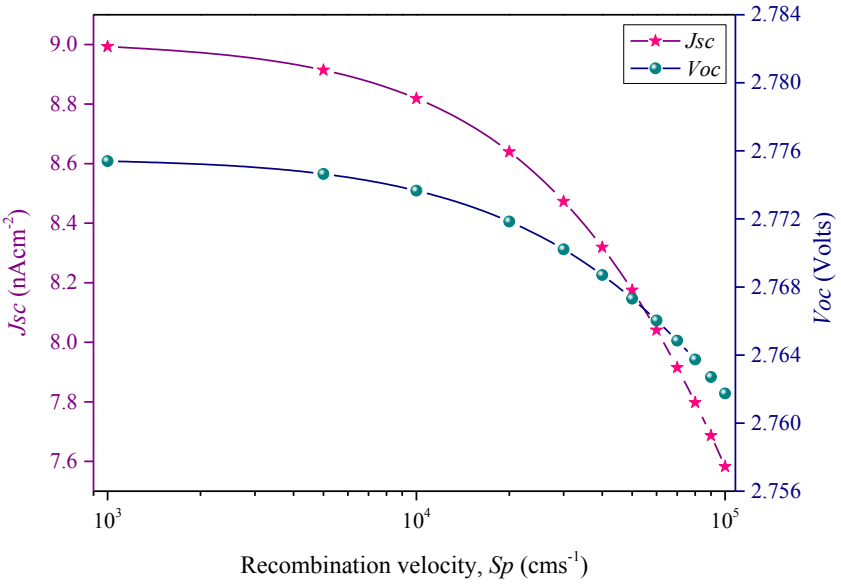

Fig. 6 Evolution of J_{sc} and V_{oc} as a function of S_p.

From Figs. 4, 5, and 6, it is evident the effect of an increasing surface recombination velocity in determining the degradation of the cell electrical performance. In more detail, we can note that the electrical parameters vary respectively from η = 23.1 %, P_{max} = 23.39 nW/cm², J_{sc} = 8.99 nA/cm², and V_{oc} = 2.77 V for $S_p = 10^3$ cm/s, to η= 19.39 %, P_{max} = 19.63 nW/cm², J_{sc} = 7.58 nA/cm², and V_{oc} = 2.76 V for $S_p = 10^5$ cm/s. As a result, we can state that the reduction of recombination phenomena on the top surface, for example by reducing the number of dangling bonds by depositing a passivating layer, may lead to a meaningful performance improvement.

4.3 Influence of the effective junction depth

The junction depth parameter, i.e. x_j in (1), plays also a key role. In this section, starting from the reference value x_j = 0.2 µm in Table 4, we simulated the $J(V)$ characteristics for 0.1≤ x_j≤ 0.5 µm assuming $S_p = 10^3$ cm/s and $N_d = N_a = 10^{16}$ cm^{-3} as shown in Fig.7. Values of x_j lower than 0.1 µm can be considered almost unrealistic for the proposed device.

https://doi.org/10.1016/j.nima.2020.164103

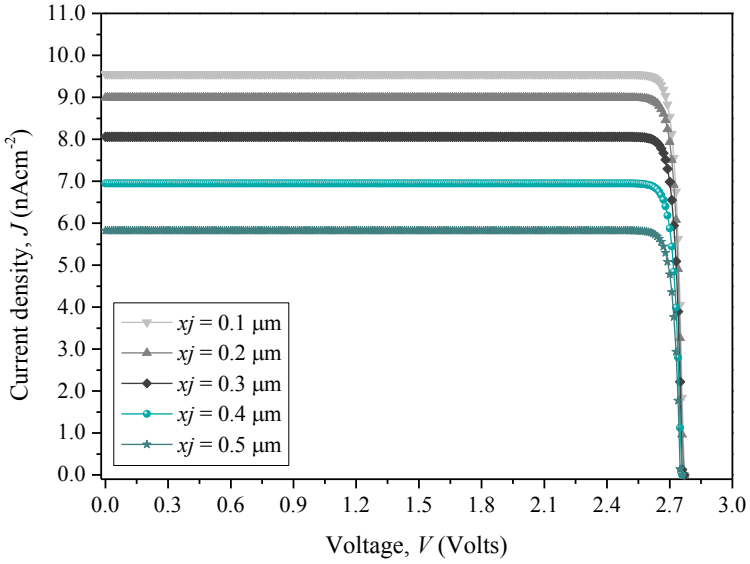

Fig. 7 Influence of the junction depth x_j on the $J(V)$ characteristics of the *GaN*-based betavoltaic cell at $T = 300$ K.

The $J(V)$ curve is deeply penalized with increasing x_j. The resulting variations of η, P_{max}, J_{sc}, and V_{oc} are shown in Figs. 8 and 9.

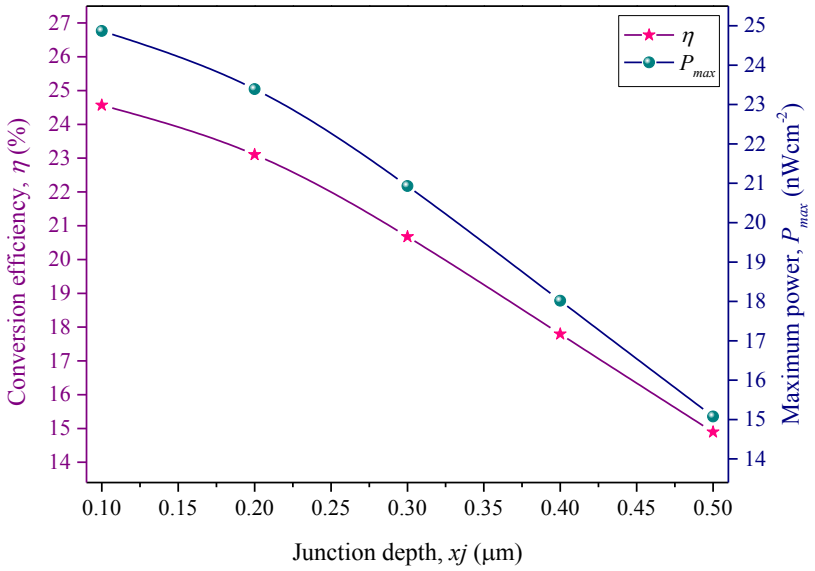

Fig. 8 Evolution of η and P_{max} as a function of x_j.

https://doi.org/10.1016/j.nima.2020.164103

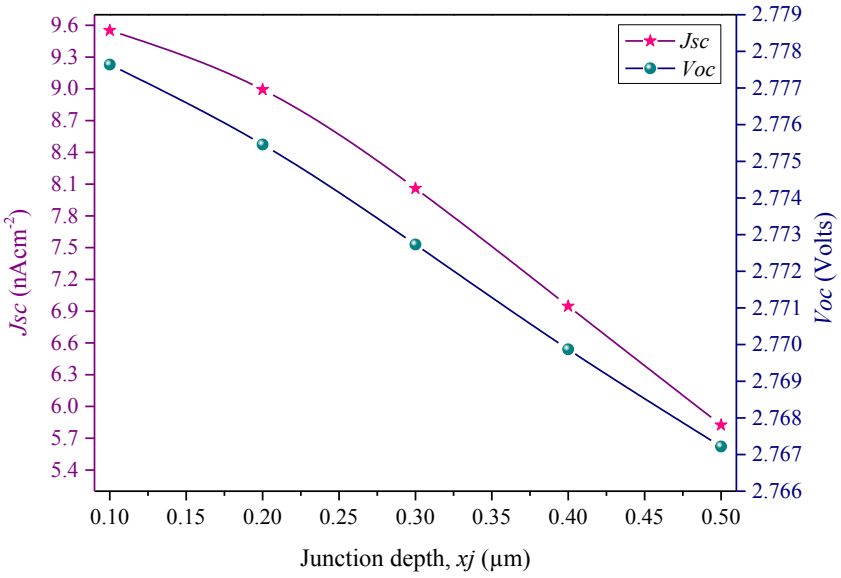

Fig. 9 Evolution of J_{sc} and V_{oc} as a function of x_j.

As we can see, P_{max} decreases from 24.87 nW/cm² for x_j = 0.1 µm to 15.07 nW/cm² for x_j = 0.5 µm, while η decreases from 24.56 % for x_j = 0.1 µm to 14.89 % for x_j = 0.5 µm. At the same time, J_{sc} and V_{oc} decreases respectively from 9.55 nA/cm² and 2.77 V for x_j = 0.1 µm to 5.82 nA/cm² and 2.76 V for x_j = 0.5 µm. The obtained results can be explained by taking into account that the increase in x_j decreases the electric field into the device structure, thus enhancing carrier recombination.

4.4 Reflection coefficient effect

The energy loss of beta-particles by reflection on the top surface greatly influences the betavoltaic cell performance. This parameter has been labelled as R in (6)-(8) and has been varied in the range 0-0.2 during the simulations, obtaining the results shown in Figs. 10-12. These results are calculated considering also the following parameters: $N_d = N_a = 10^{16}$ cm^{-3}, x_j = 0.1 µm, $S_p = 10^3$ cm/s, $S_n = 5\times10^3$ cm/s, and A = 1 mCi/cm².

https://doi.org/10.1016/j.nima.2020.164103

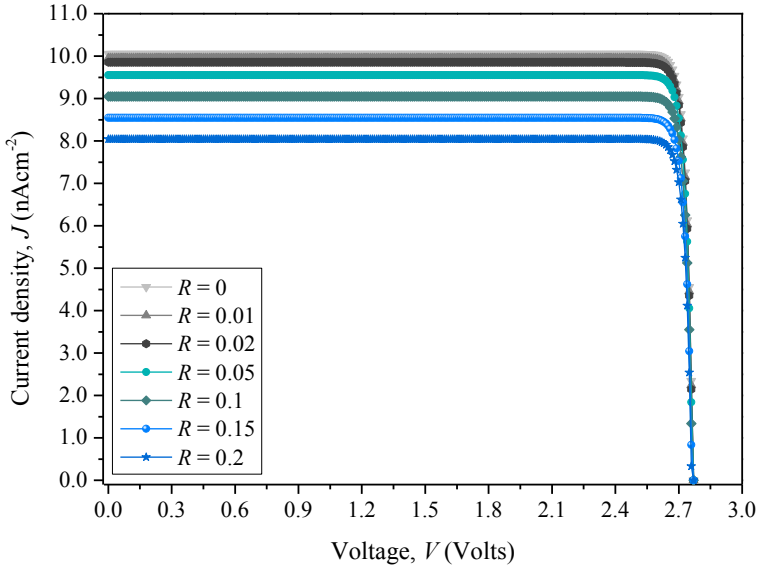

Fig. 10 Influence of the reflection coefficient R on the $J(V)$ characteristics of the *GaN*-based betavoltaic cell at $T = 300$ K.

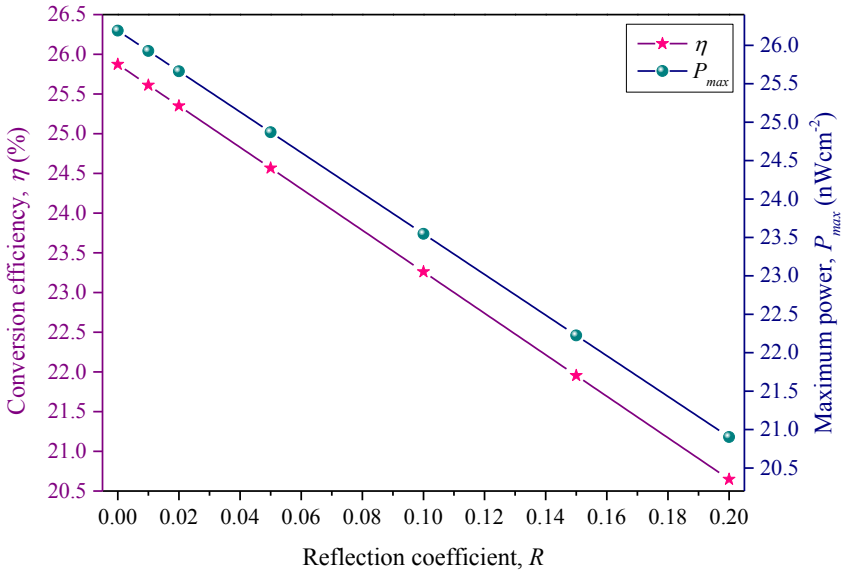

Fig. 11 Evolution of η and P_{max} as a function of R.

https://doi.org/10.1016/j.nima.2020.164103

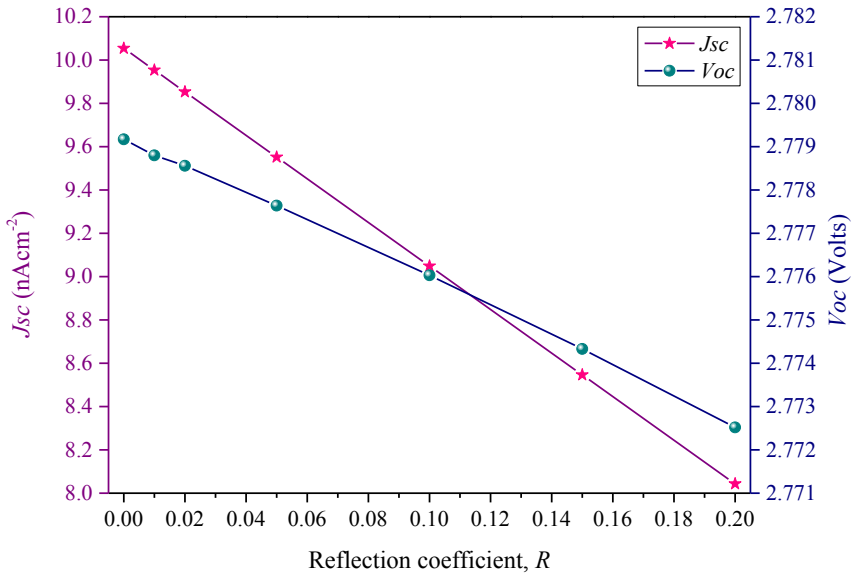

Fig. 12 Evolution of J_{sc} and V_{oc} as a function of R.

As expected, the increase of R significantly influences the $J(V)$ characteristics in Fig. 10. Also, the conversion efficiency of the cell is limited to about 20.5% when $R = 0.2$. For example, in [29] the authors assume $R = 0.1$. However, the conversion efficiency can theoretically reach 25.87% if the beta-particles reflection is eliminated. In this condition, the output parameters of the cell are $P_{max} = 26.19$ nW/cm², $J_{sc} = 10.05$ nA/cm², and $V_{oc} = 2.779$ V. Therefore, to improve the betavoltaic cell efficiency, it is necessary to limit the energy losses by reflection at the lowest possible level. This can be achieved by depositing or growing an anti-reflection layer on the top surface of the cell (surface texturing) as well as minimizing the contact area.

4.5 Radioactivity density effect

In all the simulation presented above, we adopted a radioactivity density of 1 mCi/cm². However, most of the reported experimental results are established using Ni^{63} sources with an activity density A up to about 30 mCi/cm² as in [27].

To study and evaluate the influence of changing the radioisotope activity density on the cell performance, we simulated the $J(V)$ characteristics for $1 \leq A \leq 25$ mCi/cm² assuming the other

https://doi.org/10.1016/j.nima.2020.164103

parameters as $N_d = N_a = 10^{16}$ cm^{-3}, $x_j = 0.1$ µm, $S_p = 10^3$ cm/s, $S_n = 5\times10^3$ cm/s, and $R = 0.01$.

The obtained results are shown in Figs. 13,14 and 15.

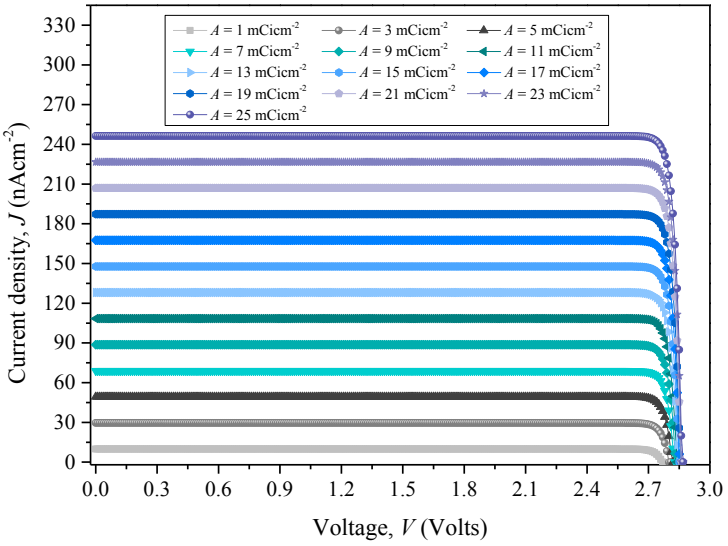

Fig. 13 Influence of the radioisotope activity density A on the $J(V)$ characteristics of the *GaN*-based betavoltaic cell at $T = 300$ K.

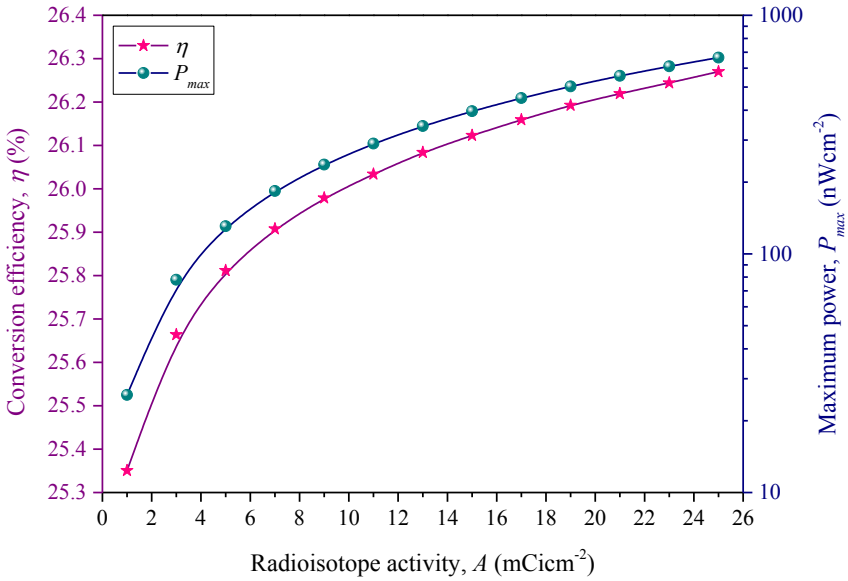

Fig. 14 Evolution of η and P_{max} as a function of A.

https://doi.org/10.1016/j.nima.2020.164103

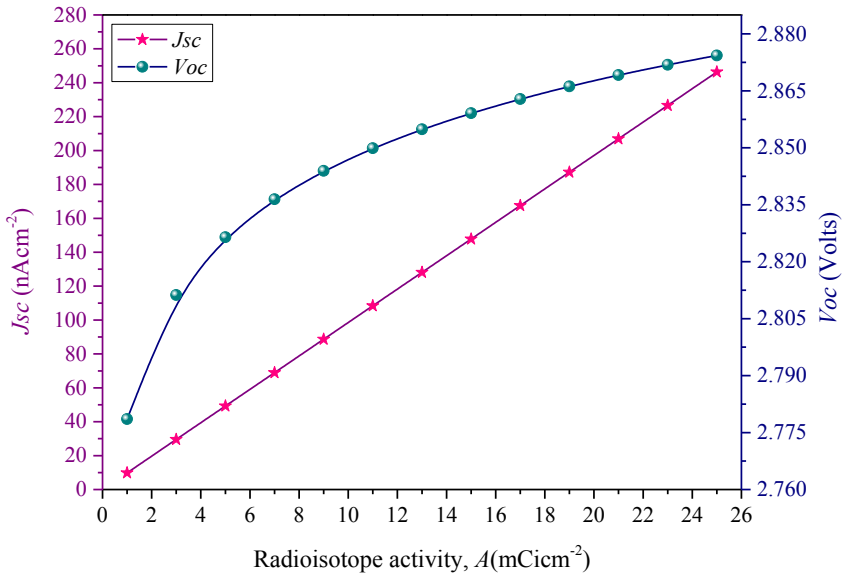

Fig. 15 Evolution of J_{sc} and V_{oc} as a function of A.

As the radioactivity density increases, both J_{sc} and V_{oc} increase. It is an expected behaviour owing to the direct proportionality that exists between J_{sc} and the beta-particles flux which is strictly dependent on A. From Fig. 14, the conversion efficiency is enhanced up to 26.27%. This value is very close to the theoretical limit of *GaN*-based betavoltaic cells. In addition, the other electrical parameters of the cell are well improved for A = 25 mCi/cm² resulting P_{max} = 660 nW/cm², J_{sc} = 240 nA/cm², and V_{oc} = 2.87 V.

5. Conclusion

In this work, we have developed a comprehensive analytical model which takes into account the fundamental physical parameters of a *GaN*-based *n*/*p* junction betavoltaic cell. The simulation results have showed that, in a device structure with a junction depth of 0.1 µm, a reflection coefficient of 0.95, and moderate doping concentrations and low levels of surface recombination velocities in both the emitter ($N_d = 1\times10^{16}$ cm^{-3}, $S_p = 1\times10^{3}$ cm/s) and the base ($N_a = 1\times10^{16}$ cm^{-3}, $S_n = 5\times10^{3}$ cm/s) regions, the adoption of a radioactive source with an activity

density of 1 mCi/cm² determines a good cell performance. In particular, the typical electrical parameters of the cell can be summarized as follows: J_{sc} = 9.55 nA/cm², V_{oc} = 2.77 V, P_{max} = 24.87 nW/cm², and η = 24.56 %. The conversion efficiency reaches the value of 26.27 % by using a radioisotope source with an activity density of 25 mCi/cm². The obtained results can turn very useful to lead the optimized design of the proposed device.

References

[1] M. Prelas, M. Boraas, F. Aguilar, J.-D. Seelig, M. T. Tchouaso, D. Wisniewski, Lecture Notes in Energy, Nuclear Batteries and Radioisotopes, Volume 56, Springer, 2016.
[2] P. Rappaport, Phys. Rev. 93 (1954) 246.
[3] Chen Hai-Yang, Jiang Lan, Li Da-Rang 2011 Chin. Phys. Lett. 28 058101.
[4] S. Butera, G. Lioliou, A.M. Barnett, Applied Radiation and Isotopes 125 (2017) 42–47.
[5] C.J. Eiting, V. Krishnamoorthy, S. Rodgers, and T. George, Appl. Phys. Lett. 88 (2006) 064101.
[6] X.-Y. Li, Y. Ren, X.-J. Chen, D.-Y. Qiao, W. -Z. Yuan, J. Radioanal Nucl. Chem. 287 (2011) 173.
[7] S. Theirrattanakul, M. Prelas, Applied Radiation and Isotopes 127 (2017) 41–46.
[8] C. Thomas, S. Portnoff, M. G. Spencer, Appl. Phys. Lett. 108 (2016) 013505.
[9] Lu, M., Wang, G., Yao, C., 2011. Gallium Nitride for nuclear batteries. Adv. Mater. Res. 343–344, 56–61.
[10] M. Lu, G.-g. Zhang, K. Fu, G.-h. Yu, D. Su, J.-f. Hu, Energy Conversion and Management 52 (2011) 1955–1958.
[11] S. Aydin, E. Kam, Investigation of nickel- 63 radioisotope- powered GaN betavoltaic nuclear battery, https://doi.org/10.1002/er.4871
[12] V.M. Andreev, A.G. Kavetskf , V.S. Kalinovsky,V.P. Khvostikov, V.R. Larionov, V.D. Rumyantsev, M.Z. Shvarts, E.V. Yakimova, V.A. Ustinov, DOI:10.1109/PVSC.2000.916117
[13] V. P. Khvostikov, V. S. Kalinovskiy, S. V. Sorokina, M. Z. Shvarts, N. S. Potapovich, O. A. Khvostikova, A. S. Vlasov, V. M. Andreev, Semiconductors 52(13) (2018) 1754–1757.
[14] C.D. Cress, B.J. Landi, R.P. Raffaelle, J Appl. Phys. 100(11) (2006) 114519.
[15] S. Butera, M.D.C. Whitaker, A.B. Krysa, A.M. Barnett, J. Phys. D: Appl. Phys. 50 (2017) 345101.
[16] M. Chandrashekhar, R. Duggirala, M.G. Spencer, A. Lal, Appl. Phys. Lett. 91 (2007) 053511.
[17] A. Krasnov, S. Legotin, K. Kuzmina, N. Ershova, B. Rogozev, A nuclear battery based on silicon p-i-n structures with electroplating ^{63}Ni layer, Nuclear Engineering and Technology (2019), doi: https://doi.org/10.1016/j.net.2019.06.003.
[18] C. Honsberg, W. A. Doolittle, M. Allen, C. Wang, Conf. Rec. 31st IEEE Photovolt. Spec. Conf. (Orlando Florida), 102-105, 2005.
[19] D.Y. Qiao, X.J. Chen, Y. Ren, W.Z. Yuan , J Microelectromech Syst. 20 (2011) 685–690.
[20] G. Hui, S. Yanqiang, Z. Yuming, Z. Yujuan, H. Jisheng, IEEE International Conference of Electron Devices and Solid-State Circuits, EDSSC 2011.

[21] M. Mohamadian, S.A.H. Feghhi, H. Afarideh, Proceedings of 13th international conference on emerging of nuclear energy systems, 2007.
[22] Z.J. Cheng, H.S. San, Z.H. Feng, B. Liu, X.Y. Chen, Electronics Letters 47 (12) (2011) 720.
[23] Z. Cheng, H. San, Y. Li, X. Chen, Proceedings of the 5th IEEE International Conference Nano/Micro Engineer. Molec. Syst, 582–586, 2010.
[24] A. A. Svintsov, A. A. Krasnov , M. A. Polikarpov, et al., Appl. Radiat Isot. 137 (2018) 184-189.
[25] T.R. Alam, M.G. Spencer, M.A. Prelas, M.A. Pierson, Int. J. Energy Res. 42 (2018) 2564–2573.
[26] R.K. Yürük, H.Tütüncüler, Canadian Journal of Physics, 97(9) (2019) 1031-1038.
[27] C. E. Munson, Q. Gaimard, K. Merghem, S. Sundaram, D. J. Rogers, J. de Sanoit, P. L. Voss, A. Ramdane, J. P. Salvestrini, A. Ougazzaden, J. Phys. D: Appl. Phys. **51** (2018) 035101. https://doi.org/10.1088/1361-6463/aa9e41
[28] Z.-J. Cheng, H.-S. San, X.-Y. Chen, B. Liu, and Z.-H. Feng, Chin. Phys. Lett. 28 (7) (2011) 078401.
[29] R. Bao, P. J. Brand, and D. B. Chrisey, IEEE Transactions on Electron Devices 59 (5) (2012).
[30] F. Bouzid, L. Dehimi, F. Pezzimenti, M. Hadjab, A.H. Larbi, Superlattice. Microst. 122 (2018) 57-73.
[31] K. Zeghdar, L. Dehimi, F. Pezzimenti, S. Rao, F.G. Della Corte, Jpn. J. Appl. Phys. 58 (2019) 014002.
[32] G. De Martino, F. Pezzimenti, F.G. Della Corte, G. Adinolfi, G. Graditi, Proc. IEEE International Conference Ph. D. Research in Microelectronics and Electronics – PRIME, 2017.
[33] F. Bouzid, F. Pezzimenti, L. Dehimi, M.L. Megherbi, F.G. Della Corte, Jpn. J. Appl. Phys. 56 (2017) 094301.
[34] Y. Marouf, L. Dehimi, F. Bouzid, F. Pezzimenti, F.G. Della Corte, Optik 163 (2018) 22.
[35] H. Bencherif, L. Dehimi, F. Pezzimenti, G. De Martino, F.G. Della Corte, J. Electron Mater. 48 (2019) 3871.
[36] G. De Martino, F. Pezzimenti, F.G. Della Corte, Proc. International Semiconductor Conference – CAS, 2018.
[37] F. Bouzid, L. Dehimi, F. Pezzimenti, J. Electron Mater. 46 (2017) 6563.
[38] H. Bencherif, L. Dehimi, F. Pezzimenti, F.G. Della Corte, Appl. Phys. A Mater. 125, (2019) 294.
[39] J. Wang, P. Mulligan, L. Brillson, L. R. Cao, Appl. Phys. Rev. 2 (2015) 031102.
[40] L.C. Olsen, Proc. 12th Space Photovoltaic Research and Technology, 256-267, 1993.
[41] C. Zerby, F. Keller, Nuclear Science and Engineering. 27(2) (1967)190-218.
[42] Z. Cheng, Z. Zhao, H. San, X. Chen, 6th IEEE International Conference on Nano/Micro Engineered and Molecular Systems, 1036-1039, 2011.
[43] S. M. Sze, K. K. Ng, Physics of Semiconductor Devices, Third Edition, John Wiley, Interscience, 2006.
[44] Y. Marouf, L. Dehimi, F. Pezzimenti, Superlattice. Microst. 130 (2019) 377.
[45] F. Bouzid, F. Pezzimenti, L. Dehimi, F.G. Della Corte, M. Hadjab, A.H. Larbi, J. Electron. Materials 48 (2019) 4107.
[46] H. Bencherif, L. Dehimi, F. Pezzimenti, F.G. Della Corte, Optik 182 (2019) 682.
[47] H. Bencherif, L. Dehimi, F. Pezzimenti, A. Yousfi, Proc. International Conference on Applied Smart Systems – ICASS, 2018.

[48] H. Teisseyre, P. Perlin, T. Suski, I. Grzegory, S. Porowski, J. Jun, J. Appl. Phys. 76 (1994) 2429.
[49] M. L. Megherbi, F. Pezzimenti, L. Dehimi, A. Saadoune, F. G. Della Corte, J. Electron. Mater. 47 (2018) 1414–1420.
[50] S. J. Pearton, C. R. Abernathy, F. Ren, Gallium Nitride Processing for Electronics, Sensors and Spintronics, Springer-Verlag, 2006.
[51] M. L. Megherbi, F. Pezzimenti, L. Dehimi, M. A. Saadoune, F. G. Della Corte, IEEE Trans. Electron Dev. 65 (2018) 3371-3378.
[52] F.G. Della Corte, G. De Martino, F. Pezzimenti, G. Adinolfi, G. Graditi, IEEE Trans. Electron Dev. 65 (2018) 3352.
[53] F. Pezzimenti, H. Bencherif, A. Yousfi, L. Dehimi, Solid-State Electron. 161 (2019) 107642.
[54] V. Bormashov, S. Troschiev, A. Volkov, S. Tarelkin, E. Korostylev, A. Golovanov, M. Kuznetsov, D. Teteruk, N. Kornilov, S. Terentiev, S. Buga, V. Blank, Phys. Status Solidi A 212(11), (2015) 2539–2547 / DOI 10.1002/pssa.201532214
[55] Alam, T.R., Pierson, M.A., 2016. Principles of betavoltaic battery design. J Energy Power Sources 3 (1), 11–41.
[56] A. Waris, Y. Kusumawati, A. S. Alfarobi, I. K. Aji, K. Basar, AIP Conference Proceedings 1719, 030053 (2016); https://doi.org/10.1063/1.4943748